Hindawi
Wireless Communications and Mobile Computing
Volume 2021, Article ID 9965727, 8 pages
https://doi.org/10.1155/2021/9965727

WILEY | Hindawi

Research Article

An Efficient Improved OGWSBI Algorithm for Accurate Off-Grid DOA Estimation of Coherent Signals

Xiangjun Xu,[1] **Mingwei Shen**,[1] **Di Wu**,[2] **and Daiyin Zhu**[2]

[1]*College of Computer and Information Engineering, Hohai University, Nanjing, China*
[2]*Key Laboratory of Radar Imaging and Microwave Photonics & Ministry of Education, Nanjing University of Aeronautics and Astronautics, Nanjing, China*

Correspondence should be addressed to Mingwei Shen; smw_hhu1981@163.com

Received 11 March 2021; Revised 6 April 2021; Accepted 28 July 2021; Published 16 September 2021

Academic Editor: Zhipeng Cai

The performance of the weighted sparse Bayesian inference (OGWSBI) algorithm for off-grid coherent DOA estimation is not satisfactory due to the inaccurate weighting information. To increase the estimation accuracy and efficiency, an improved OGWSBI algorithm based on a higher-order off-grid model and unitary transformation for off-grid coherent DOA estimation is proposed in this paper. Firstly, to reduce the approximate error of the first-order off-grid model, the steering vector is reformulated by the second-order Taylor expansion. Then, the received data is transformed from complex value to real value and the coherent signals are decorrelated via utilizing unitary transformation, which can increase the computational efficiency and restore the rank of the covariance matrix. Finally, in the real field, the steering vector higher-order approximation model and weighted sparse Bayesian inference are combined together to realize the estimation of DOA. Extensive simulation results indicate that under the condition of coherent signals and low SNR, the estimation accuracy of the proposed algorithm is about 50% higher than that of the OGWSBI algorithm, and the calculation time is reduced by about 60%.

1. Introduction

Direction-of-arrival (DOA) estimation is a basic problem in array signal processing and one of the crucial tasks in radar, sonar, and other fields [1, 2]. During the development of DOA estimation technology, a host of methods have been proposed. The classical DOA estimation algorithms based on subspace technique, such as MUSIC algorithm [3] and ESPRIT algorithm [4], have been widely applied and improved. Since these subspace-based algorithms all rely on accurate representation of the signal subspace and noise subspace, their estimation performance will be seriously reduced in low SNR and coherent signals.

In recent years, the compressed sensing (CS) signal processing method [5, 6] has captured the growing attention of scholars thus leading to its wide application in various fields. In view of the sparsity of the array model, scholars apply the CS theory to DOA estimation and proposed a sea of sparsity-driven methods [7–9], the most successful of which is L1-SVD [10]. Compared with subspace DOA estimation algorithms, the sparse representation methods exhibit many advantages, e.g., improved robustness to noise, limited number of snapshots, and correlation of signals [11]. However, these methods employ a fixed sampling grid and can achieve outstanding performance only if all the true DOAs are exactly lying on the sampling grid points. Nevertheless, in practice, this assumption is virtually impossible. Usually, we use an off-grid gap to represent the gap between the true DOA and its nearest grid point.

To tackle the estimation error caused by an off-grid gap, recently, scholars have done a lot of research on the off-grid DOA estimation and proposed a number of improved algorithms [12–15]. The most representative one is the off-grid sparse Bayesian inference (OGSBI) algorithm proposed by Yang et al. [16], which achieves high-precision DOA estimation under coarse grid conditions. On the basis of the OGSBI algorithm, Zhang et al. proposed the weighted sparse Bayesian inference (OGWSBI) algorithm [17]. By utilizing the hyperprior of the source signals obtained from the weighted vector, OGWSBI has better performance than OGSBI in

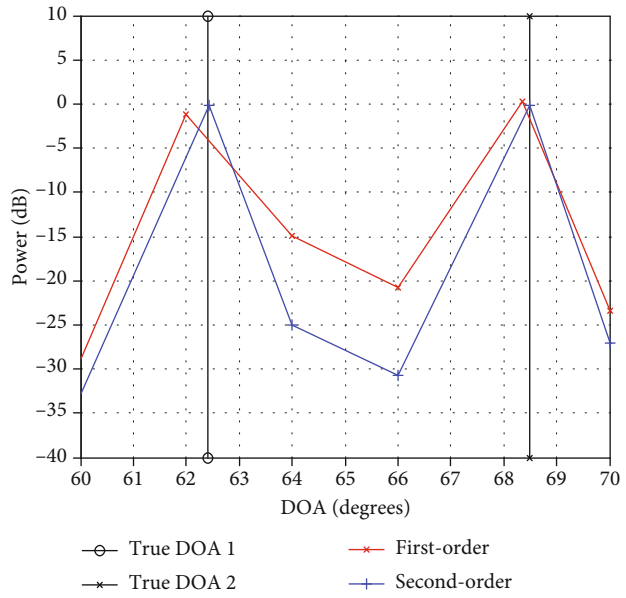

Figure 1: OGWSBI estimated incoherent signal angle profile.

terms of DOA estimation precision and convergence. However, the weighted vector is constructed by the MUSIC algorithm. Therefore, on the conditions of coherent signals, the estimation accuracy of the OGWSBI will be seriously reduced due to the inaccurate weighting information.

In this paper, we propose an improved algorithm of OGWSBI that applies to coherent signal cases. The proposed algorithm is termed as improved off-grid weighted sparse Bayesian inference (IOGWSBI). We apply a unitary transformation of the received data to achieve decoherence and increase computational efficiency. In addition, to further improve the estimation accuracy, we expand the steering vector from first-order approximation to second-order approximation. Simulation results show that compared with the OGWSBI algorithm, the proposed algorithm has obvious improvements in accuracy and efficiency.

2. Performance Analysis of OGWSBI

OGWSBI is an improved off-grid DOA estimation algorithm from a Bayesian perspective based on OGSBI, which has an outstanding performance in terms of off-grid DOA estimation. Nevertheless, on the one hand, the estimation accuracy of OGWSBI will be degraded due to the absence of higher-order Taylor expansion terms of the steering vector. As shown in Figure 1, the OGWSBI algorithm can obtain higher estimation accuracy under the higher-order approximation model of the steering vector when the incoherent angles are 62.4° and 68.5° , the number of snapshot is 100, and SNR = 20 dB.

First-order denotes first-order Taylor expansion of the steering vector based on OGWSBI, and second-order denotes second-order Taylor expansion of the steering vector based on OGWSBI.

On the other hand, since the MUSIC estimator has "high resolution" and "universal adaptability," OGWSBI exploits these abilities of MUSIC to construct a weighted vector to provide a priori information of spatial distribution for algorithm iteration. Therefore, OGWSBI can improve the estimation accuracy and convergence speed when the source signals are incoherent. However, when the source signals are coherent, the signal subspace and the noise subspace cannot be correctly represented, resulting in a rapid decrease in the performance of the MUSIC algorithm, and the weighting coefficient cannot be represented correctly. Thus, the performance of the OGWSBI algorithm decreases rapidly. Figure 2 is the angle profile of the OGWSBI algorithm under incoherent and coherent conditions when the incident angles are 72.6° and 94.5°, the number of snapshot is 100, and SNR = 10 dB.

As shown in Figure 2, when the signals are incoherent, OGWSBI can accurately estimate the source angle. However, when the signals are coherent, the estimation accuracy decreases rapidly, and the source angle cannot be effectively estimated.

According to the above performance analysis, the estimation accuracy and convergence speed of the OGWSBI algorithm can be improved effectively through the higher-order off-grid approximation model and unitary transformation. Therefore, in what follows next, these two aspects are carefully expatiated.

3. Principle of IOGWSBI

3.1. Second-Order Taylor Expansion of the Off-Grid Model. Suppose that K narrowband far-field sources whose angles are $\theta_1, \theta_2, \cdots \theta_K$ impinging on a uniform linear array (ULA) constituted by M omnidirectional receiving sensors. The signal wavelength is λ, and the distance between adjacent array elements is $d = \lambda/2$. Assuming there are L snapshots, then array output data can be expressed as

$$\mathbf{Y} = \mathbf{AS} + \mathbf{N}, \tag{1}$$

where $\mathbf{Y} = [\mathbf{Y}(1), \cdots, \mathbf{Y}(L)] \in \mathbb{C}^{M\times L}$ is the vector of the received data, $\mathbf{N} = [\mathbf{N}(1), \cdots, \mathbf{N}(L)] \in \mathbb{C}^{M\times L}$ is the measurement noise, $\mathbf{S} \in \mathbb{C}^{N\times L}$, N denotes the grid number, and $\mathbf{A} = [\mathbf{a}(\theta_1), \cdots, \mathbf{a}(\theta_N)] \in \mathbb{C}^{M\times N}$ is the overcomplete basis matrix.

In order to tackle the problem of estimation error caused by an off-grid gap, the off-grid model is introduced for the DOA estimation. Let $\widehat{\theta} = \{\widehat{\theta}_1, \cdots, \widehat{\theta}_N\}$ be a fixed sampling set which uniformly covers the entire DOA range $[0, \pi]$. We define the true direction $\theta_k \in \{\theta_1, \cdots, \theta_K\}$ and the nearest grid point $\widehat{\theta}_{n_k} \in \{\widehat{\theta}_1, \cdots, \widehat{\theta}_N\}$. The steering vector $\mathbf{a}(\theta_K)$ is approximated by employing linearization:

$$\mathbf{a}(\theta_k) \approx \mathbf{a}\left(\widehat{\theta}_{n_k}\right) + \mathbf{b}\left(\widehat{\theta}_{n_k}\right)\left(\theta_k - \widehat{\theta}_{n_k}\right) + 0.5 * \mathbf{c}\left(\widehat{\theta}_{n_k}\right)\left(\theta_k - \theta\wedge_{n_k}\right)^2, \tag{2}$$

where $\mathbf{b}(\widehat{\theta}_{n_k}) = \mathbf{a}^{'}(\widehat{\theta}_{n_k})$, $\mathbf{c}(\widehat{\theta}_{n_k}) = \mathbf{a}^{\prime\prime}(\widehat{\theta}_{n_k})$, the true overcomplete basis matrix can be redefined as

$$\mathbf{\Phi}(\boldsymbol{\beta}) = \mathbf{A} + \mathbf{B}\ \mathrm{diag}\ (\boldsymbol{\beta}) + 0.5 * \mathbf{C} * \mathrm{diag}\left(\boldsymbol{\beta}^{\wedge^2}\right), \tag{3}$$

with $\mathbf{A} = [\mathbf{a}(\widehat{\theta}_1), \cdots, \mathbf{a}(\widehat{\theta}_N)]$, $\mathbf{B} = [\mathbf{b}(\widehat{\theta}_1), \cdots, \mathbf{b}(\widehat{\theta}_N)]$, $\mathbf{C} = [\mathbf{c}$

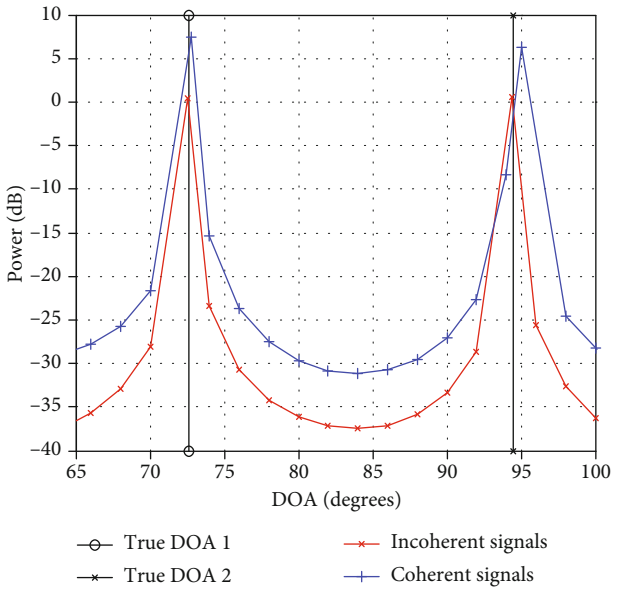

Figure 2: Incoherent and coherent signal angle profile.

$(\widehat{\theta}_1), \cdots, \mathbf{c}(\widehat{\theta}_N)]$, the off-grid sparse representation of (1) can be redefined as

$$\mathbf{Y} = \mathbf{\Phi}(\boldsymbol{\beta})\mathbf{S} + \mathbf{N}. \tag{4}$$

Equation (4) is an off-grid DOA estimation model based on the second-order Taylor expansion of the steering vector. Through this model, the signal fitting error is reduced compared with the first-order Taylor expansion model of the steering vector, thereby improving the estimation accuracy. This model is suitable for scenarios with high estimation accuracy, such as cruise missiles and vehicle positioning.

3.2. Unitary Transformation of the Estimation Model. When the source signals are coherent, it will cause the rank deficiency of the source covariance matrix and the divergence of the signal feature vector from the noise subspace. The key to processing the DOA estimation of coherent signals is to restore the rank of the covariance to be consistent with the number of signal sources. This processing method is called decorrelation. Among them, the unitary transformation of the estimation model is one of the decorrelation algorithms.

If the matrix $A \in \mathbb{C}^{M\times N}$ is centrohermitian [18], the specific expression of the unitary transformation is

$$\mathbf{A}_\mathbf{r} = \mathbf{U}_M^H \mathbf{A} \mathbf{U}_N, \tag{5}$$

where $\mathbf{A}_\mathbf{r}$ denotes the real value (RV) matrix, and $\mathbf{U}$ is the unitary matrix. When M is even, we have

$$\mathbf{U}_M = \frac{1}{\sqrt{2}} \begin{bmatrix} \mathbf{I} & j\mathbf{I} \\ \mathbf{J} & -j\mathbf{J} \end{bmatrix}, \tag{6}$$

with the size of $\mathbf{I}$ and $\mathbf{J}$ being $M/2 \times M/2$. $\mathbf{I}$ is the identity matrix, $\mathbf{J}$ is the switching matrix whose counter-diagonal is 1, and the other elements are 0. When M is odd, we have

$$\mathbf{U}_M = \frac{1}{\sqrt{2}} \begin{bmatrix} \mathbf{I} & \mathbf{0} & j\mathbf{I} \\ 0 & \sqrt{2} & 0 \\ \mathbf{J} & \mathbf{0} & -j\mathbf{J} \end{bmatrix}. \tag{7}$$

Here, $\mathbf{I}$ and $\mathbf{J}$ are matrices that have the dimension of $(M-1)/2$.

According to (5), the unitary transformation takes advantage of the characteristics of the centrohermitian matrix to transform, so it is necessary to construct an augmented matrix to transform the received data of the array into the centrohermitian matrix. If receiving signal $\mathbf{Y} \in \mathbb{C}^{M\times L}$, then, the augmented matrix is constructed as

$$\mathbf{Y}_{\text{aug}} = [\mathbf{Y} \vdots \mathbf{J}_M \mathbf{Y}^* \mathbf{J}_L], \tag{8}$$

with $\mathbf{Y}_{\text{aug}} \in \mathbb{C}^{M\times 2L}$. The received signal in the real field $\mathbf{Y}'$ can be obtained by (5).

Then, the corresponding transformation of the overcomplete basis matrix can be expressed as

$$\begin{aligned} \mathbf{A} &= \left[\mathbf{U}_M \mathbf{a}\left(\widehat{\theta}_1\right), \mathbf{U}_M \mathbf{a}\left(\widehat{\theta}_2\right) \cdots, \mathbf{U}_M \mathbf{a}\left(\widehat{\theta}_N\right)\right], \\ \mathbf{B} &= \left[\mathbf{U}_M \mathbf{b}\left(\widehat{\theta}_1\right), \mathbf{U}_M \mathbf{b}\left(\widehat{\theta}_2\right) \cdots, \mathbf{U}_M \mathbf{b}\left(\widehat{\theta}_N\right)\right], \\ \mathbf{C} &= \left[\mathbf{U}_M \mathbf{c}\left(\widehat{\theta}_1\right), \mathbf{U}_M \mathbf{c}\left(\widehat{\theta}_2\right) \cdots, \mathbf{U}_M \mathbf{c}\left(\widehat{\theta}_N\right)\right]. \end{aligned} \tag{9}$$

If covariance matrix $\mathbf{R} = E[\mathbf{y}_{\text{aug}}(t)\mathbf{y}_{\text{aug}}^H(t)]$, then covariance matrix $\mathbf{R}_{fb}$ under the forward/backward spatial smoothing algorithm satisfies

$$\mathbf{R}_{fb} = \frac{1}{2}(\mathbf{R} + \mathbf{J}_M \mathbf{R}^* \mathbf{J}_M) = \frac{1}{2L} \mathbf{Y}_{\text{aug}} \mathbf{Y}_{\text{aug}}{}^H. \tag{10}$$

According to (5), the received signal $\mathbf{Y}_{\text{aug}}$ is subjected to unitary transformation: $\mathbf{Y}' = \mathbf{U}_M^H \mathbf{Y}_{\text{aug}} \mathbf{U}_{2L}$. Then, the covariance matrix of the received signal after unitary transformation is expressed as

$$\begin{aligned} \mathbf{R}' &= \frac{1}{2L} \mathbf{Y}' \left(\mathbf{Y}'\right)^H = \frac{1}{2L} \mathbf{U}_M^H \mathbf{Y}_{\text{aug}} \mathbf{U}_{2L} \left(\mathbf{U}_M^H \mathbf{Y}_{\text{aug}} \mathbf{U}_{2L}\right)^H \\ &= \frac{1}{2L} \mathbf{U}_M^H \mathbf{Y}_{\text{aug}} \mathbf{U}_{2L} \mathbf{U}_{2L}{}^H \mathbf{Y}_{\text{aug}}{}^H \mathbf{U}_M = \frac{1}{2L} \mathbf{U}_M^H \mathbf{Y}_{\text{aug}} \mathbf{Y}_{\text{aug}}{}^H \mathbf{U}_M. \end{aligned} \tag{11}$$

According to (10) and (11), the covariance matrix $\mathbf{R}'$ can be expressed as

$$\mathbf{R}' = \mathbf{U}_M^H \mathbf{R}_{fb} \mathbf{U}_M. \tag{12}$$

From (12) and the forward and backward smoothing algorithm, it can be seen that the unitary transformation of the estimation model can be used for decorrelation

processing, that is, when the signal sources are coherent signals, the rank of the covariance matrix is restored to the number of sources, thus rank $(\mathbf{R}') = K$.

As shown in Figure 3, two angles of 62° and 82° unequal power coherent signals are incidents on a uniform linear array with 8 elements, the distance between the elements is half a wavelength, and the MUSIC algorithm is used for DOA estimation. It can be found that without decorrelation processing, the signal subspace and noise subspace cannot be correctly represented, resulting in false peaks or underestimation. The estimation performance of the MUSIC algorithm drops rapidly. However, after the unitary transformation is used for decorrelation processing, with the restoration of the covariance matrix rank, the signal subspace and the noise subspace are correctly represented, so the MUSIC algorithm can recover the incident angle of the signal with high accuracy.

In addition, the unitary transformation can further improve the computational efficiency of the algorithm. Therefore, the unitary transformation processing of the estimation model not only can perform decorrelation processing but can also reduce the calculation time.

3.3. Weighted Sparse Bayesian Formulation. The OGWSBI algorithm bases on a weighted vector constructed via the MUSIC algorithm. To reduce the complexity of the algorithm and obtain the signal subspace $\mathbf{U}_s$ and the noise subspace $\mathbf{U}_e$, the algorithm utilizes a singular value decomposition approach, and the column dimension of $\mathbf{Y}'$ and $\mathbf{S}$ are reduced from L to K. The inverted MUSIC space spectrum formula is expressed as [17]

$$w_n = \mathbf{a}^H\left(\widehat{\theta}_n\right)\mathbf{U}_e\mathbf{U}_e{}^H\mathbf{a}\left(\widehat{\theta}_n\right) n = 1, 2, \cdots N, \tag{13}$$

where $\boldsymbol{w} = [w_1, \cdots, w_N]^T$ denotes the weighted vector. However, weighting only requires the "discrimination" between different signals, that is, where there is a signal, a small weighting coefficient is used, and where there is no signal, a large weighting coefficient is used. Therefore, the normalization of (13) can be expressed as

$$\mathbf{w} = \frac{\mathbf{w}}{\min(\mathbf{w})}. \tag{14}$$

Further, we assume that the noise follows a circular Gaussian distribution with mean zero, variance $\sigma^2 I_M$, and $\alpha_0 = \sigma^{-2}$ which represent the noise precision. This leads us to the expression:

$$\boldsymbol{p}\left(\mathbf{Y}' \mid \mathbf{S}, \boldsymbol{\alpha}_0, \boldsymbol{\beta}\right) = \prod_{t=1}^{K} \boldsymbol{\mathcal{CN}}\left(\mathbf{y}'(t) \mid \boldsymbol{\Phi}(\boldsymbol{\beta})\mathbf{s}(t), \boldsymbol{\alpha}_0^{-1}\mathbf{I}\right). \tag{15}$$

Based on the statistical assumption of incident signal $\mathbf{S}$, we assume it follows a two-stage hierarchical prior with independent snapshots denoted as $p(\mathbf{S}; \rho) = \int p(\mathbf{S} \mid \boldsymbol{\alpha}) p(\boldsymbol{\alpha}; \rho) d\boldsymbol{\alpha}$, $\rho > 0$, $\boldsymbol{\alpha} \in \mathfrak{R}^N$, $\boldsymbol{\Lambda} = \text{diag}(\boldsymbol{\alpha})$, and

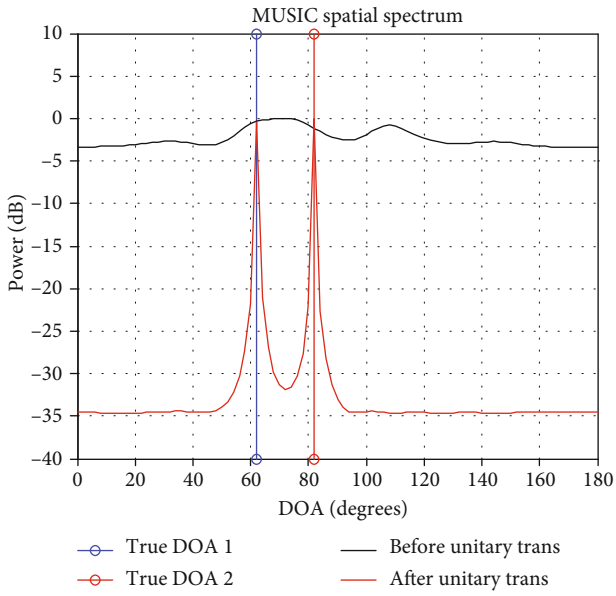

Figure 3: MUSIC estimated coherent signal angle profile.

$$p(\mathbf{S} \mid \boldsymbol{\alpha}) = \prod_{t=1}^{K} \mathcal{CN}(\mathbf{s}(t) \mid 0, \boldsymbol{\Lambda}),$$
$$p(\boldsymbol{\alpha}; \rho) = \prod_{n=1}^{N} \Gamma(\alpha_n \mid 1, w_n\rho), \tag{16}$$

where $\boldsymbol{\alpha}$ denotes the variance of signal.

According to D.MacKay's research, the posterior probability distribution $p(\mathbf{S}, \alpha_0, \boldsymbol{\alpha}, \boldsymbol{\beta} \mid \mathbf{Y}')$ cannot be solved directly. However, another form of posterior probability distribution of $\mathbf{S}$ can be expressed as

$$p\left(\mathbf{S} \mid \mathbf{Y}', \alpha_0, \boldsymbol{\alpha}, \boldsymbol{\beta}\right) = \prod_{t=1}^{K} \mathcal{CN}(\mathbf{s}(t) \mid \boldsymbol{\mu}(t), \boldsymbol{\Sigma}), \tag{17}$$

with $\boldsymbol{\mu}(t) = \alpha_0\boldsymbol{\Sigma}\boldsymbol{\Phi}^H y'(t), t = 1, \cdots, K$, $\boldsymbol{\Sigma} = (\alpha_0\boldsymbol{\Phi}^H\boldsymbol{\Phi} + \boldsymbol{\Lambda}^{-1})^{-1}$, $\boldsymbol{\mu}(t)$ is the signal mean, and $\boldsymbol{\Sigma}$ is the signal covariance matrix. The update formula of $\alpha_0, \boldsymbol{\alpha}$ can be written as

$$\alpha_n = \frac{\left(\sqrt{K^2 + 4w_n\underline{\rho}\left(\left(\left\|\underline{\boldsymbol{\mu}}^n\right\|_2^2 + \Sigma_{nn}\right)\right)} - K\right)}{2w_n\underline{\rho}}, \quad n = 1, 2, \cdots, N,$$
$$\alpha_0 = \frac{MK + b - 1}{\left(\left(\left\|\underline{\mathbf{Y}'} - \Phi\underline{\boldsymbol{\mu}}\right\|_F^2 + \alpha_0^{-1}\sum_{n=1}^{N}\gamma_n\right) + c\right)}, \tag{18}$$

where $\underline{\mathbf{Y}'} = \mathbf{Y}'/\sqrt{K}$, $\underline{\boldsymbol{\mu}} = \boldsymbol{\mu}/\sqrt{K}$, $\underline{\boldsymbol{\rho}} = \boldsymbol{\rho}/K$, $\gamma_n = 1 - \alpha_n^{-1}\Sigma_{nn}$, $b \longrightarrow 0, c \longrightarrow 0$.

According to [16], for $\boldsymbol{\beta}$, its estimate maximizes $E\{\log p(\mathbf{Y}' \mid \mathbf{S}, \alpha_0, \boldsymbol{\beta}) p(\boldsymbol{\beta})\}$ and minimizes

$$\begin{aligned} & E\left\{\frac{1}{T}\sum_{t=1}^{K}\left\|\mathbf{y}'(t)-\left(\mathbf{A}+\mathbf{B}\ \mathrm{diag}\ (\boldsymbol{\beta})+0.5\mathbf{C}\ \mathrm{diag}\left(\boldsymbol{\beta}_{\cdot}^{\wedge^2}\right)\right)\mathbf{s}(t)\right\|_2^2\right\} \\ & =\frac{1}{K}\sum_{t=1}^{K}\left\|\mathbf{y}'(t)-\left(\mathbf{A}+\mathbf{B}\ \mathrm{diag}\ (\boldsymbol{\beta})+0.5\mathbf{C}\ \mathrm{diag}\left(\boldsymbol{\beta}_{\cdot}^{\wedge^2}\right)\right)\mathbf{u}(t)\right\|_2^2 \\ & +Tr\left\{\left(\mathbf{A}+\mathbf{B}\ \mathrm{diag}\ (\boldsymbol{\beta})+0.5\mathbf{C}\ \mathrm{diag}\left(\boldsymbol{\beta}_{\cdot}^{\wedge^2}\right)\right)\boldsymbol{\Sigma}\left(\mathbf{A}+\mathbf{B}\ \mathrm{diag}\ (\boldsymbol{\beta})+0.5\mathbf{C}\ \mathrm{diag}\left(\boldsymbol{\beta}_{\cdot}^{\wedge^2}\right)\right)^H\right\}, \end{aligned} \tag{19}$$

where the specific solution of $\boldsymbol{\beta}$ can be referenced to [19]. Different from the OGSBI algorithm, Yang et al. gave the specific solution process of the $\boldsymbol{\beta}$ under the steering vector higher-order approximate model.

Finally, the termination condition of the iteration is that $\|\boldsymbol{\alpha}^{i+1}-\boldsymbol{\alpha}^{i}\|_2/\|\boldsymbol{\alpha}^{i}\|_2 < \tau$ or the maximum number of iterations *imax* is reached, where i denotes the number of iterations and τ is the predefined tolerance parameter. The specific algorithm flow chart is shown in Figure 4.

4. Simulation Results

In order to further analyze the performance of the unitary transformation and the higher-order approximation of the steering vector, in the following simulations, we first put together the unitary transformation and the OGWSBI algorithm to obtain a RV-OGWSBI algorithm. Thereafter, the performance of the OGSBI, OGWSBI, and RV-OGWSBI algorithms are compared by simulations. Then, the steering vector is expanded from the first-order approximation to the second-order approximation, and the performance of the IOGWSBI and RV-OGWSBI algorithms is simulated and analyzed.

In the following simulations, a uniform linear array of $M = 8$ sensors with $d = \lambda/2$ and 100 Monte Carlo trials are simulated. The grid interval is set to be $r = 2^0$, and two coherent signals are simulated with directions 64.8° and 86.5°. We initialize $\alpha = (1/MK)\sum_{t=1}^{K}|\mathbf{A}^H(\mathbf{Y}')_t|$, $\alpha_0 = 1$. We set $\rho = 0.01$, $c = d = 10^{-4}$, $\tau = 10^{-3}$, and the maximum number of the iterations to be 2000.

4.1. Performance Analysis of RV-OGWSBI

4.1.1. DOA Estimation Spatial Spectrum. In the first experiment, the number of snapshots and SNR are fixed at $L =$ 100 and 10 dB. The following simulation compares the DOA estimation spatial spectrum of the three algorithms of OGSBI, OGWSBI, and RV-OGWSBI.

Figure 5 shows the spatial spectrum comparison of the OGSBI, OGWSBI, and RV-OGWSBI algorithm proposed in this paper in a Monte Carlo experiment. From the observation of Figure 5, we can see that RV-OGWSBI has better performance than OGSBI and OGWSBI in the case of coherent signals. The estimated angles are given in Table 1.

4.1.2. RMSE of DOA Estimation. The next two experiments verify the performance improvement of the proposed algorithm (RV-OGWSBI) in terms of the root-mean-square error (RMSE) of DOA estimation. Figure 6 shows the RMSE of DOA estimation versus SNR based on 100 snapshots. Figure 7 shows the RMSE of DOA estimation versus number of snapshots, with SNR fixed at 10 dB. Based on these two simulations, it is shown that the RV-OGWSBI can get better performance than OGWSBI, since the decoherence of signals as well as the correct weighting cofficient. In addition, it is also observed that RV-OGWSBI outperforms OGSBI under the same simulation condition.

4.1.3. Computational Time. Regarding the computational complexity of the iteration process, OGWSBI and RV-OGWSBI have a computational complexity of order $O(\max(MN^2))$. However, in the case of coherent sources, due to the accurate weighted prior information, the number of iterations of RV-OGWSBI is much smaller than that of OGWSBI. In addition, by utilizing a unitary transformation to obtain a real-value response of the complex-valued matrix, it increases the computational efficiency. Therefore, the RV-OGWSBI algorithm is noted to be more efficient than the OGWSBI algorithm.

Figure 8 shows the total CPU time versus SNR based on 100 snapshots. As can be seen from the figure, the computational time of all algorithms decreases with the increase of SNR. Under the same conditions, the computational efficiency of RV-OGWSBI is about 65% higher than that of OGWSBI. Another observation is that the running time of RV-OGWSBI is also lower than that of OGSBI.

4.2. Performance Analysis of IOGWSBI. In order to further improve the estimation accuracy of the algorithm, the application scenarios of the algorithm are further expanded. Based on the proposed algorithm RV-OGWSBI, the first-order Taylor expansion of the steering vector is extended to the second-order Taylor expansion, so as to reduce the modeling error caused by mismatch. The comparative simulation analysis is shown as follows.

4.2.1. RMSE of DOA Estimation. Figure 9 shows the RMSE of DOA estimation versus SNR based on 100 snapshots. Figure 10 shows the RMSE of DOA estimation versus number of snapshots, with SNR fixed at 10 dB. Based on these

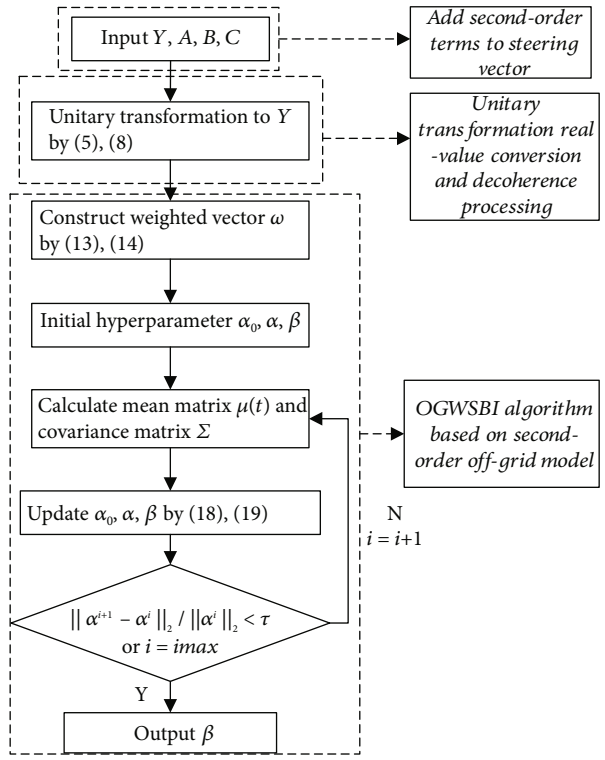

Figure 4: Flow chart of the proposed algorithm.

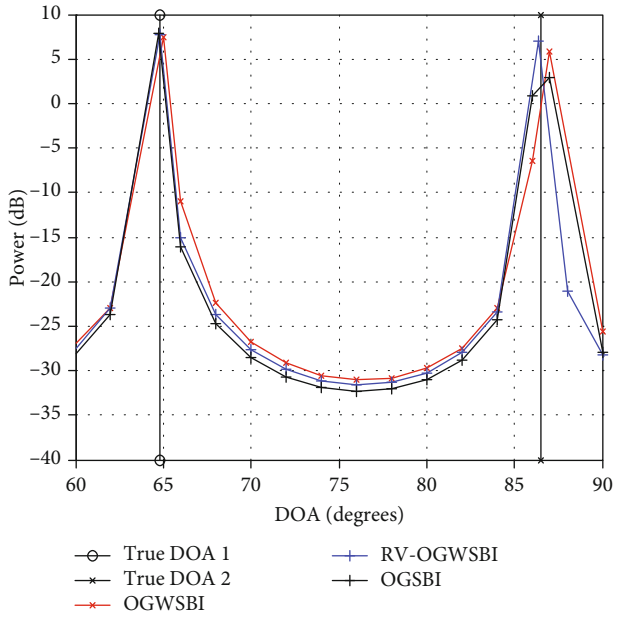

Figure 5: Comparison of the spatial spectrum.

two simulations, the RMSE of the two algorithms gradually decreases as the SNR and the number of snapshots increase. However, the IOGWSBI algorithm improves the off-grid model and reduces the fitting error of the signal. Therefore, it is also observed that IOGWSBI has better performance compared with RV-OGWSBI under the same simulation condition. In addition, the estimation accuracy of the

Table 1: Estimated angles.

	θ_1	θ_2
True signals	64.8°	86.5°
OGSBI	64.76°	87°
OGWSBI	65°	87°
RV-OGWSBI	64.77°	86.38°

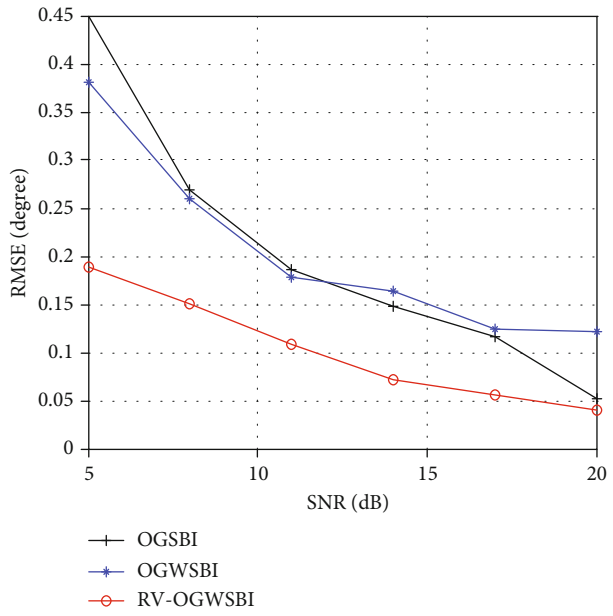

Figure 6: RMSE of DOA estimation versus SNR.

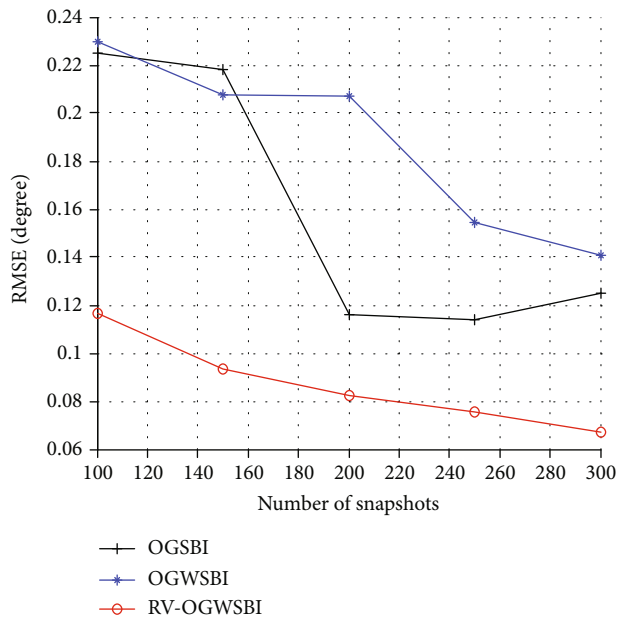

Figure 7: RMSE of DOA estimation versus the number of snapshots.

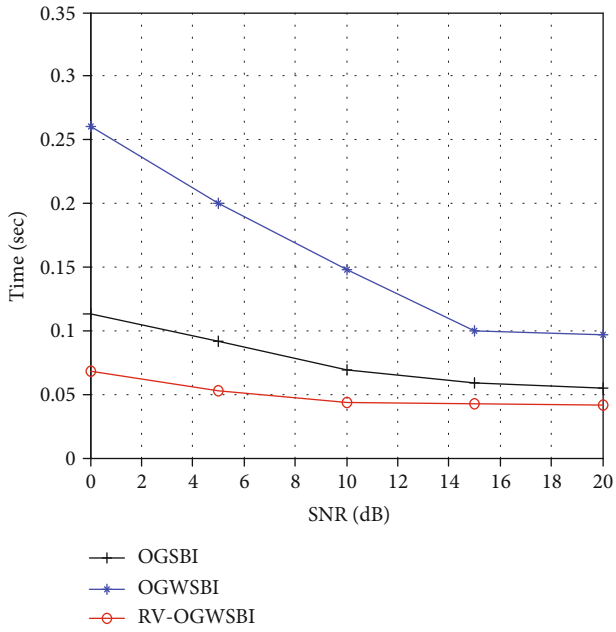

Figure 8: Computational time versus SNR.

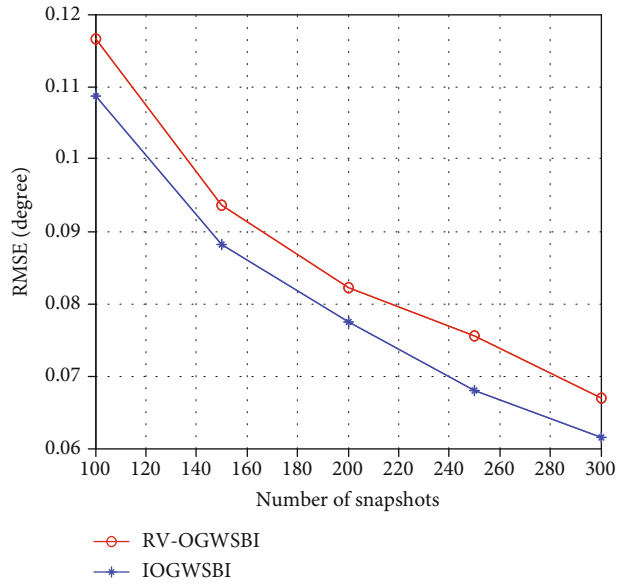

Figure 10: RMSE of DOA estimation versus the number of snapshots.

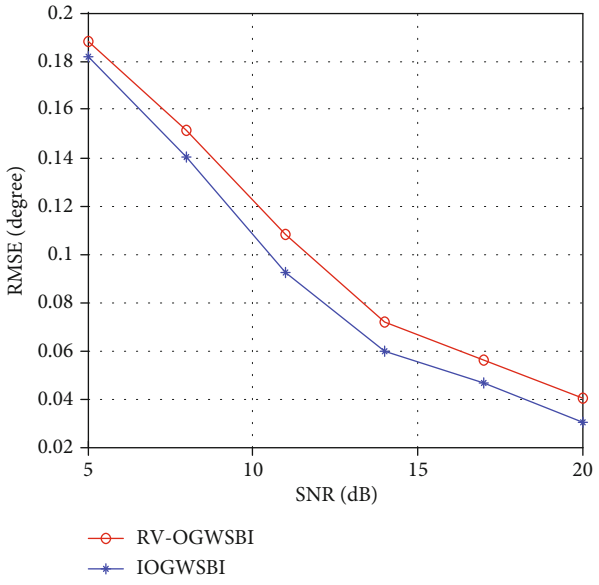

Figure 9: RMSE of DOA estimation versus SNR.

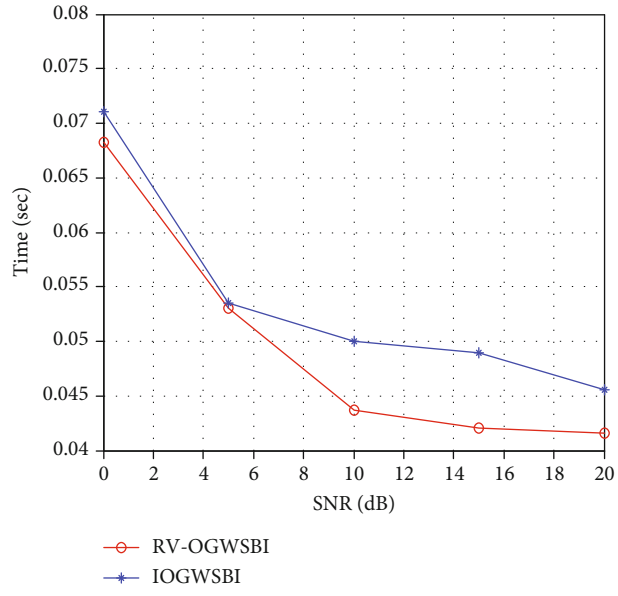

Figure 11: Computational time versus SNR.

IOGWSBI algorithm is about 50% higher than that of the OGWSBI algorithm.

4.2.2. Computational Time. Figure 11 shows the total CPU time versus SNR based on 100 snapshots. As can be seen from Figure 11, when the SNR varies from 0 to 20 dB, the computational time of the two algorithms decreases continuously with the increase of the SNR. Due to the higher-order approximation of the steering vector, the computational efficiency of IOGWSBI is lower than that of RV-OGWSBI. However, compared to OGWSBI, the computational efficiency of IOGWSBI is still increased by 60%. Therefore, under the condition of coherent sources, the IOGWSBI algorithm maintains an efficient and high-precision off-grid DOA estimation performance, which is more suitable for scenarios with higher accuracy requirements.

5. Conclusion

OGWSBI presents enormous advantages in off-grid DOA estimation when the signals are incoherent when compared with OGSBI. This is due to OGWSBI weighted vector exploitation which provides priori information of the spatial distribution to improve the efficiency and estimation accuracy of

the algorithm. However, the problem is that the algorithm can not estimate coherent signals effectively which thus lead to a reduction of its practical application. Therefore, our proposed algorithm devises a unitary transformation mechanism and real value conversion to attain signal decoherence, improve estimation accuracy, and reduce computational time. Furthermore, in order to further improve the estimation accuracy, a higher-order approximation model of the steering vector is constructed. Simulation experiments conducted verify the accuracy and efficiency of the proposed algorithm. In addition, the practical application scenarios of the weighted sparse Bayesian algorithm have been broadened.

Data Availability

All the data generated or analyzed in this study are available from the corresponding author on reasonable request.

Conflicts of Interest

The authors declare that they have no conflicts of interest.

Acknowledgments

This work was supported in part by the National Natural Science Foundation of China (No. 61771182 and No. 41830110) and the Fundamental Research Funds for the Central Universities (No. B210202076).

References

[1] Q. Wang, Z. Zhao, Z. Chen, and Z. Nie, "Grid evolution method for DOA estimation," *IEEE Transactions on Signal Processing*, vol. 66, no. 9, pp. 2374–2383, 2018.

[2] H. Krim and M. Viberg, "Two decades of array signal processing research: the parametric approach," *IEEE Signal Processing Magazine*, vol. 13, no. 4, pp. 67–94, 1996.

[3] E. Claudio, R. Parisi, and G. Jacovitti, "Space time MUSIC: consistent signal subspace estimation for wideband sensor arrays," *IEEE Transactions on Signal Processing*, vol. 66, no. 10, pp. 2685–2699, 2018.

[4] J. J. Pan, M. Sun, Y. D. Wang, and X. F. Zhang, "An enhanced spatial smoothing technique with ESPRIT algorithm for direction of arrival estimation in coherent scenarios," *IEEE Transactions on Signal Processing*, vol. 68, pp. 3635–3643, 2020.

[5] D. Donoho, "Compressed sensing," *IEEE Transactions on Information Theory*, vol. 52, no. 4, pp. 1289–1306, 2006.

[6] Z. H. Wei, L. Yang, Z. H. Wang, B. C. Zhang, Y. Lin, and Y. R. Wu, "Wide angle SAR subaperture imaging based on modified compressive sensing," *IEEE Sensors Journal*, vol. 18, no. 13, pp. 5439–5444, 2018.

[7] X. Wang, M. Huang, and L. Wan, "Joint 2D-DOD and 2D-DOA estimation for co-prime EMVS-MIMO radar," *Circuits, Systems, and Signal Processing*, vol. 1, pp. 1–17, 2021.

[8] E. Baidoo, J. Hu, B. Zeng, and B. D. Kwakye, "Joint DOD and DOA estimation using tensor reconstruction based sparse representation approach for bistatic MIMO radar with unknown noise effect," *Signal Processing*, vol. 182, article 107912, 2021.

[9] X. Wang, L. T. Yang, D. D. Meng, M. X. Dong, K. Ota, and H. F. Wang, "Multi-UAV cooperative localization for marine targets based on weighted subspace fitting in SAGIN environment," *IEEE Internet of Things Journal*, pp. 1–11, 2021.

[10] D. Malioutov, M. Cetin, and A. Willsky, "A sparse signal reconstruction perspective for source localization with sensor arrays," *IEEE Transactions on Signal Processing*, vol. 53, no. 8, pp. 3010–3022, 2005.

[11] J. S. Dai, X. Bao, W. C. Xu, and C. Q. Chang, "Root sparse Bayesian learning for off-grid DOA estimation," *IEEE Signal Processing Letters*, vol. 24, no. 1, pp. 46–50, 2017.

[12] H. Zhu, G. Leus, and G. B. Giannakis, "Sparsity-cognizant total least-squares for perturbed compressive sampling," *IEEE Transactions on Signal Processing*, vol. 59, no. 5, pp. 2002–2016, 2011.

[13] Y. Zhang, Z. Ye, X. Xu, and N. Hu, "Off-grid DOA estimation using array covariance matrix and block-sparse Bayesian learning," *Signal Processing*, vol. 98, pp. 197–201, 2014.

[14] P. Chen, Z. Cao, Z. Chen, and X. Wang, "Off-grid DOA estimation using sparse Bayesian learning in MIMO radar with unknown mutual coupling," *IEEE Transactions on Signal Processing*, vol. 67, no. 1, pp. 208–220, 2019.

[15] E. Baidoo, J. Hu, and L. Zhan, "Kalman filtering method for sparse off-grid angle estimation for bistatic multiple-input multiple-output radar," *IET Radar, Sonar & Navigation*, vol. 14, no. 2, pp. 313–319, 2020.

[16] Z. Yang, L. Xie, and C. Zhang, "Off-grid direction of arrival estimation using sparse Bayesian inference," *IEEE Transactions on Signal Processing*, vol. 61, no. 1, pp. 38–43, 2013.

[17] Y. Zhang, Z. Ye, and X. Xu, "Off-grid direction of arrival estimation based on weighted sparse Bayesian learning," in *2014 International Conference on Audio, Language and Image Processing*, pp. 547–550, Shanghai, China, 2015.

[18] N. Yilmazer, J. Koh, and T. K. Sarkar, "Utilization of a unitary transform for efficient computation in the matrix pencil method to find the direction of arrival," *IEEE Transactions on Antennas and Propagation*, vol. 54, no. 1, pp. 175-176, 2006.

[19] J. Yang, G. S. Liao, and J. Li, "An efficient off-grid DOA estimation approach for nested array signal processing by using sparse Bayesian learning strategies," *Signal Processing*, vol. 128, pp. 110–122, 2016.